Analytica Chimica Acta 1203 (2022) 339722

Contents lists available at ScienceDirect

Analytica Chimica Acta

journal homepage: www.elsevier.com/locate/aca

Microfluidic aptasensor POC device for determination of whole blood potassium

Chin-Chung Tseng [a, b, 1], Song-Yu Lu [c, 1], Szu-Jui Chen [c, 1], Ju-Ming Wang [d], Lung-Ming Fu [c, *], Yi-Hong Wu [c]

[a] Division of Nephrology, Department of Internal Medicine, National Cheng Kung University Hospital Dou-Liou Branch, College of Medicine, National Cheng Kung University, Yunlin, 640, Taiwan
[b] Department of Internal Medicine, National Cheng Kung University Hospital, College of Medicine, National Cheng Kung University, Tainan, 701, Taiwan
[c] Department of Engineering Science, National Cheng Kung University, Tainan, 701, Taiwan
[d] Department of Biotechnology and Bioindustry Sciences, National Cheng Kung University, Tainan, 701, Taiwan

HIGHLIGHTS

- A microfluidic aptasensor POC device is proposed for monitoring the K^+ ions in CKD patients.
- The device comprises of a PMMA/paper-microchip and a RGB analysis system.
- The K^+ ion concentration in the 287 real-world CKD serum samples was measured.
- The measurement results are in good agreement ($R^2 = 0.980$) with the ISE method.

GRAPHICAL ABSTRACT

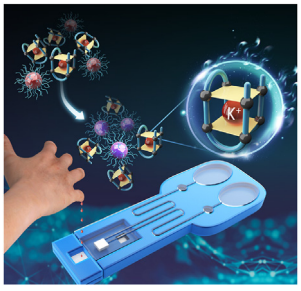

ARTICLE INFO

Article history:
Received 23 October 2021
Received in revised form
7 February 2022
Accepted 10 March 2022
Available online 14 March 2022

Keywords:
CKD
Microfluidic
Microchip
Paper-based biosensor
Blood potassium ion
Aptamer

ABSTRACT

An integrated microfluidic Au nanoparticle (AuNP) aptasensor device is proposed for monitoring the concentration of potassium (K^+) ions in the bloodstream of patients with chronic kidney disease (CKD). In the proposed detection device, the AuNPs in the AuNP/aptamer complex are displaced by the serum K^+ ions and react with NaCl to produce a color change in the detection region from which the K^+ ion concentration is then inversely derived. The microfluidic device comprises two main components, namely an AuNP aptasensor PMMA (Poly(methyl methacrylate))/paper-microchip and a colorimetric analysis system for the quantitative detection of K^+ ion concentration in whole blood. The functions of PMMA/paper microchips include reagent storage, K^+ ion/aptamer reaction, and separation of serum from whole blood samples (blood filter). Experimental results show that the microfluidic device provides a linear response over the K^+ ion concentration in range of 0.05–9 mM in artificial serum and has a detection limit (LOD) of 0.01 mM. Moreover, the detection results obtained for the 137 whole blood and 287 serum samples of CKD patients are very consistent ($R^2 = 0.968$ and $R^2 = 0.980$) with the measurement results obtained using an ion-selective electrodes (ISE) method. Results confirm that the current microfluidic aptasensor device provides a highly-sensitive and convenient method for performing the point-of-care (POC) monitoring of the whole blood K^+ ion concentration.

* Corresponding author.
E-mail address: loudyfu@mail.ncku.edu.tw (L.-M. Fu).
[1] These authors contributed equally to this paper.

https://doi.org/10.1016/j.aca.2022.339722
0003-2670/

1. Introduction

Potassium (K^+) ions are the most abundant ion in the human body and play a vital role in controlling muscle and nerve activity, maintaining body fluid levels, and performing various other important functions. For healthy human adults, the normal value of human serum K^+ ions lies in the range of 3.5–5.5 mM (mEq/L). High K^+ concentrations may cause fatigue or weakness, numbness or tingling, nausea or vomiting, difficulties breathing, chest pain, and irregular heart rhythm. In extreme cases, excessive K^+ ions may cause paralysis, heart failure, or even sudden death [1]. By contrast, low K^+ ion concentrations (referred to medically as hypokalemia) may cause cramps, weakness, malaise, myalgia, and various other symptoms. Furthermore, severe hypokalemia can lead to potentially fatal conditions, such as hypotension, arrhythmia, and tachycardia [2–5]. Therefore, CKD patients should pay attention to the choice of diet and avoid high-potassium and high-phosphorus foods. If the diet is not restrained and intake of a diet rich in K^+ ions, it may have serious consequences due to hyperkalemia. Although some of the K^+ ions can be removed by hemodialysis for CKD patients undergoing dialysis, the K^+ ions in the blood will gradually accumulate with the food intake of each meal. In other words, CKD patients have the highest blood K^+ concentration and the most dangerous before the next dialysis, so the monitoring of K^+ ions in the blood of CKD patients is very important.

The serum K^+ concentration is particularly important for Chronic Kidney Disease (CKD) patients since excessive or insufficient K^+ levels place the patient at an increased risk of mortality. Therefore, selective and sensitive K^+ ion sensors are essential in facilitating the effective diagnosis and treatment of CKD patients. Many measurement methods for the determination of K^+ ions have been developed, including Raman scattering spectroscopy (RSS), electrochemical (EC) sensing, atomic absorption spectrophotometry (AAS), ion selective electrodes (ISE), ion chromatography (IC), and so on [5–10]. However, most of these methods require complicated instruments and tedious laboratory procedures. Furthermore, most of them also have the shortcomings of narrow detection ranges, relatively high detection limits and the inability to perform real-time detection. Therefore, there is an urgent need for a new platform that can detect serum K^+ ions in a more rapid, convenient, low-cost and effective manner.

Microfluidic technology, with a high integration ability and good biocompatibility, provides outstanding detection advantages for many biomedicine, environmental and food science applications [11–15]. As microfluidics technology has evolved, many "lab-on-a-chip" devices have been proposed for performing reagent mixing, separation, analysis and detection functions on a single platform [16–20]. Generally speaking, these microfluidic systems [21–25] can be classified as either microfluidic chip-based devices [26–30] or microfluidic paper-based analysis devices (μPADs) [31–35]. Both systems offer many advantages over conventional benchtop devices, including smaller sample volume, rapider response time, higher portability, and reduced reagent consumption [36–40]. However, of the two systems, μPADs are more qualified for point-of-care testing (POCT) due to their lower cost, easier fabrication, and simpler operation [41–48]. Cai et al. [49] developed a μPAD based on the field amplification stacking (FAS) effect for performing the enhanced-sensitivity detection of microalbuminuria (MAU) in urine samples. It was shown that the stacking effect increased the concentration of fluorescein isothiocyanate-labeled bovine serum albumin (FITC-BSA) in artificial urine samples by more than 100-fold. Moreover, by staining the protein stacking band with bromophenol blue (BPB), the device achieved a linear detection range for human serum albumin (HSA) of 10–300 mg/L with a limit of detection (LOD) of 4.9 mg/L. Various researchers have shown that the sensitivity and specificity of μPAD detection platforms can be further improved through the combination of metal nanoparticles [50–53] and aptamer sensors [54–56].

This study proposes a microfluidic aptasensor device for the rapid measurement of whole blood K^+ ions in CKD patients. The microfluidic device comprises an AuNP aptasensor PMMA/paper-microchip and a colorimetric detection system. The detection method is based on the adsorption of cationic molecules caused by NaCl, which neutralizes the surface charge of AuNPs and produces the aggregation of AuNPs (Fig. S1(a)) [57]. In particular, an AuNP aptasensor is prepared by adsorbing a specific aptamer sequence on the surface of AuNPs (Fig. S1(b)). When K^+ ions are subsequently added, the aptamer sequence binds to the ions and produces a four-strand structure compound (G-quartet) through the hydrogen bonds formed between the guanines. The formation of the rigid G-quadruplex structure reduces the electrostatic force acting on the AuNPs and causes them to detach from the surface of the aptasensor (Fig. S1(c)). In the presence of NaCl, the repulsion force between the detached AuNPs is reduced, and hence the AuNPs aggregate and produce a color change of the AuNP/aptamer + NaCl reaction product. For a constant NaCl concentration, a higher K^+ ion concentration results in a greater detachment and agglomeration of the AuNPs and hence leads to a lighter color. By contrast, for a lower K^+ ion concentration, a smaller number of AuNPs are detached, and hence a more minor color change occurs. Consequently, the K^+ ion concentration can be quantitatively determined by observing the color change of the detection zone of the paper chip following the injection of the serum sample into the PMMA/paper-based device.

2. Experimental details

2.1. Synthesis of AuNPs, aptamer and AuNP aptasensor

The AuNPs were synthesized via a liquid-phase chemical reduction method [58]. Gold(III) chloride trihydrate solution (250 mL, 1 mM, Alfa Aesar Co., U.S.A) was added to an Erlenmeyer flask and heated under continuous magnetic stirring until it reached boiling temperature. 25 mL of 38.8 mM sodium citrate (Avantor Inc., U.S.A.) was rapidly added to the boiling gold(III) chloride trihydrate solution and the solution was heated for a further 15 min; resulting in a gradual color change from golden yellow (Au^{3+}) to transparent (Au^{2+}), black (Au^+), and finally wine red (AuNPs). The synthesized AuNPs were found to have a size of 17.6 nm (Fig. S2) and an absorption peak of 524 nm, as determined by a dynamic light scattering particle size analyzer (Nanoptic 90, Bettersize, U.S.A.) and UV–vis light spectrometer (G10S, Thermo Fisher Scientific Taiwan Co., Taiwan), respectively.

Aptamer sequence 5′-TTT GGT TGG TGT GGT TGG TTT-3 was purchased from Protech Technology Enterprise Co., Ltd., Taiwan. A 100 μM aptamer stock solution was prepared using secondary sterilized water (104 μL). The solution was aliquoted into 2-μL centrifuge tubes and stored in a refrigerator at −20 °C. 1 mL of the AuNP solution was added to a tube with 1 μL aptamer (100 μM) and shaken gently to obtain a uniform dispersion. The solution was then left to stand for 5 min to allow the aptamers to be adsorbed on the surface of the AuNPs under the effects of electrostatic force. As the aptamers were adsorbed on the AuNP surface, the surface charge increased; resulting in a negative repulsive force between the particles and a uniform dispersion of the AuNPs in the solution without aggregation.

2.2. Manufacturing and assembly of PMMA/paper-microchip

Fig. 1 shows the complete structure of the proposed PMMA/paper-microchip, which consists of a reagent chip and a whole

blood filter chip. As shown in Fig. 1(a), the reagent chip consists of a sealing film layer with a thickness of 0.1 mm, two PET (polyethylene terephthalate) cover layers with a thickness of 0.1 mm, a paper-chip, and two PMMA layers (one is the reagent storage and finger pump layer, and the other is the sliding structure layer) with a thickness of 0.4 mm. The whole blood filter chip consists of two PET with a thickness of 0.2 mm and a PMMA substrate with a thickness of 0.4 mm. The patterns of the reagent chip and the whole blood filter chip were fabricated by a CO_2 laser processing machine (Taiwan Giant Technology Co., Ltd.) using an unfocused laser beam method, and a smooth channel wall can be obtained without an annealing process. (The detailed information of laser processing is provided in previous studies [59,60] and are hence omitted here.)

The reagent chip (see Fig. 1(a) and (c)) contains two reagent tanks (Reagent B, aptamer, circular diameter 2 mm; and Reagent C, NaCl, circular diameter 2 mm); and two finger pump tanks (ellipse diameter 15 × 6 mm^2) connected to the detection zone (2 × 2 mm^2) by microchannels with a width and depth of 200 μm and 100 μm, respectively. The whole blood filter chip (see Fig. 1(b) and (c)) contains a waste chamber (2 × 2 × 0.2 mm^3), a rectangular sample chamber (4 × 4 × 0.6 mm^3), and square paper-chip detection zone (2 × 2 × 0.2 mm^3) connected by a filtration/separation micro-channel with sample chamber. After the laser ablation process, the reagent chip and the whole blood filter chip were individually bonded under the conditions of a maximum pressure of 10 kg/cm^2 and a temperature of 100 °C for 12 min. After the bonding process, the reagent chip is filled with reagents B and C (aptamers; 0.5 μL, 100 μM; NaCl; 3 μL, 0.6 M), and then sealed with a sealing film. The blood filter chip is implanted with reagent-coated AuNPs (reagent A, 8 μL) paper-chip (Advantec filter paper No. 1, Japan) and a paper strip (blood separation membrane, Fr1, Advanced Microdevices Ltd., India) into the detection zone and filtration/separation microchannel, respectively. Fig. 1(b) shows the cross-sectional structure of whole blood filter chip and describes the process of separating a whole blood sample into serum and transferring it to the reaction zone. Finally, the whole blood filter chip was inserted into the reagent chip to integrate the PMMA/paper-microchip. The PMMA/paper-microchip was then stored at 4 °C in a nitrogen environment until required for use. Note that the maximum storage time was determined to be 60 days (Fig. S3).

2.3. Detection system

As shown in Fig. S4, the main components of the sample pre-treatment and detection system included a 12 V/5 V power supply (RID-85A, Tun-Hwa Elec. Co., Taiwan), two relays, a buck converter, a temperature controller (PXR-4, Fuji Co., Japan) for temperature control and display, an image analysis box for captured composite image, a WiFi chip (Arduino D1 WiFi, Taiwan) for transmitting captured image, a voltage switch and voltage adjustment button for voltage detection and controller, a fan (DF8015UB, JetArt Tech. Co., Taiwan) for system cooling, and a smart phone for analyzed the color intensity. The image analysis box contained an LED (light-emitting diode) light source, a voltage controller, a CMOS (complementary metal-oxide semiconductor) camera (1080 × 1920 pixels, Taiwan Dmatek Co. Ltd.), a chip holder, a hotplate and a connector.

2.4. Materials and methods

A stock K^+ ion solution with a concentration of 1 M was prepared by mixing Roche automation system calibration solution powder (Roche Co., Germany) with 3000 μL of deionized (DI) water. The solution was then further diluted with DI water to obtain artificial serum samples with K^+ ion concentrations of 0.05, 1, 3, 6 and 9 mM, respectively. Samples for UV spectrometer characterization were prepared by adding 1 mL of AuNP solution and 1 μL aptamer (100 μM) to cuvettes and shaking gently to obtain a uniform dispersion. The solutions were then allowed to stand for 5 min to allow the aptamer to be adsorbed on the surface of the AuNPs. The artificial K^+ ion samples (10 μL) were added to the cuvettes and left to stand for a further 10 min. Finally, NaCl (10 μL, 600 mM) was

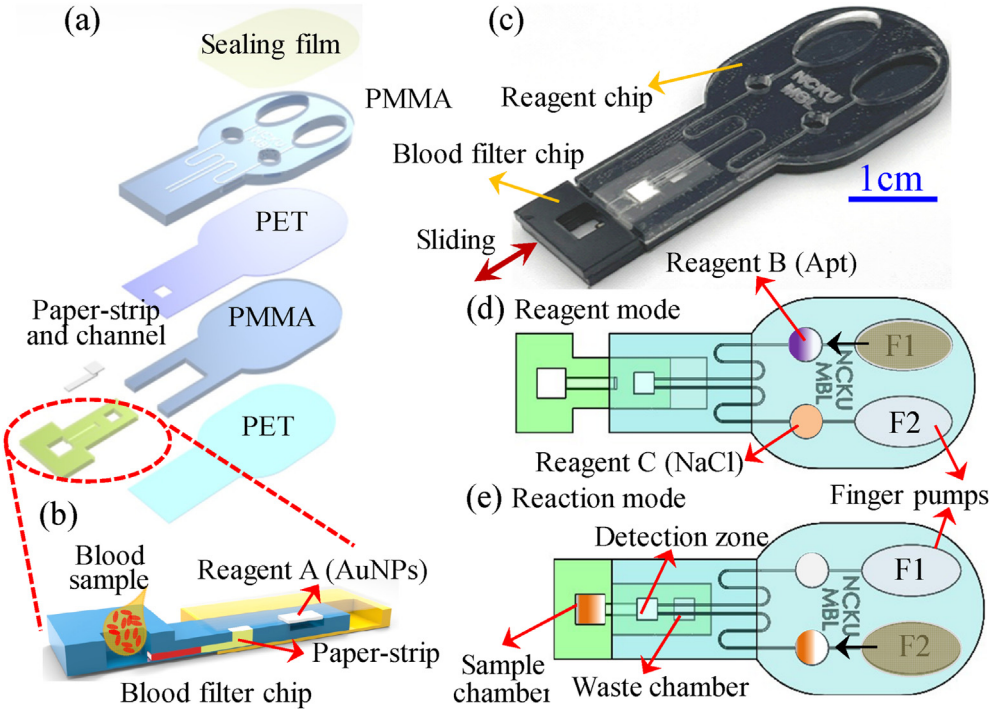

Fig. 1. Schematic illustration and photograph of PMMA/paper-microchip.

added to the solution as an agglomeration agent and shaken gently to produce a uniform dispersion. Finally, the absorbance of the K^+ ions was measured with a spectrophotometer at a wavelength of 530 nm. For a more detailed description of macroscale serum K^+ Ion detection using spectrophotometry technique, please refer to section S.1 of the supplementary material.

In performing the microfluidic detection process, the PMMA/paper-microchip was switched to the reagent mode (see Fig. 1(d)). The finger pump (F1) was then used to deliver Reagent B (aptamer) to the detection zone. After waiting for 2 min for the aptamer to bind with AuNPs, the excess aptamer will flow into the waste chamber. 3 μL whole blood sample was injected to sample chamber, and then PMMA/paper-microchip was switched to reaction mode (sample target reacts with AuNP/aptamer, see Fig. 1(e)). A further 3 min was allowed for the whole blood to be separated into serum, and the K^+ ions in the serum to react with the AuNP/aptamer to form a compact rigid G-quadruplex structure. Then, the second finger pump (F2) was activated to drive the reagent C (NaCl) to the detection zone to facilitate a colorimetric reaction. Finally, the paper chip was inserted into the image analysis box and activate the light source. The resulting images collected by the CMOS camera were transferred wirelessly to a smart phone and the K^+ ion concentration was then used self-developed RGB analysis app. A more details about the operation of the RGB color code APP software has been shown in our previous study [38]. Fig. 2 shows the operating steps of the experimental procedure.

3. Results and discussion

3.1. Serum K^+ ion detection using microfluidic aptasensor device

To determine the optimal K^+ ion detection conditions for the proposed microfluidic aptasensor device, a series of preliminary experiments was performed using different volumes and concentrations of the various reagents (AuNPs, NaCl, Apt). Fig. 3(a) shows the detection zone of the paper-based chip for various volumes of AuNPs and concentrations of NaCl (3 μl). As shown, in the absence of NaCl, the detection zone has a bright red appearance; particularly at higher AuNP volumes. However, as the NaCl concentration increases, the color of the detection zone changes from bright red to purple-red, and finally blue-gray. Since red and blue-gray span two different color levels in the RGB color space, a single color appears when detecting the RGB intensity of the detection zone, and hence the resolution of the detection process is degraded. To avoid this phenomenon, the optimal detection condition was thus specified as that which resulted in a pure blue-gray (i.e., no red) color of the detection zone. Consequently, the optimal AuNP and NaCl conditions were chosen as 8 μL AuNPs and 3 μL NaCl with a concentration of 0.4 M, as shown in Fig. 3(a).

As mentioned earlier, the main purpose of the aptamers in the present study is to protect the AuNPs from aggregation and combine with the K^+ ions to produce a G-quadruplex structure. The presence of excessive aptamers prevents the release of AuNPs from the aptasensor following the introduction of K^+ ions, and therefore limits the colorimetric reaction with the NaCl. By contrast, the absence of sufficient aptamers fails to suppress the aggregation of the AuNPs, and therefore also results in detection errors. Fig. 3(b) shows the color of the detection zone in the paper-based chip given the use of 8 μL AuNPs, 3 μL NaCl (0.4 M), and various volumes of aptamers. It is seen that the optimal color level is obtained when using an aptamer volume of 0.4 μL.

To ensure the reliability of the color detection process, K^+ ion samples with concentrations of 0.05–10 mM were injected into the PMMA/paper-based device under fixed parameter conditions of 8 μL AuNPs, 0.4 μL aptamer and 3 μL NaCl (0.4 M). Fig. 4(a) presents the corresponding RGB intensity values of the detection zone after the colorimetric reaction. The results show that the green and blue intensity values increase linearly with an increasing K^+ ion concentration. However, the red intensity value exhibits a significant discontinuity at a K^+ ion concentration of 3 mM. The main reason for the discontinuity of the "R" value is that the color of the detection zone changes from bright red to purplish-red. Accordingly, the higher NaCl concentration of 0.6 M was used to focus the reaction color in the purple-red region and the experiments were repeated. In this case, all three intensity values increase linearly and continuously over the considered K^+ ion concentration range, as shown in Fig. 4(b). Furthermore, the average determination coefficient (R^2) is greater than 0.98 for every color signal. Thus, the final reagent conditions for all of the remaining experiments were set as 8 μL AuNPs, 0.4 μL Apt and 3 μL NaCl (0.6 M).

Fig. 5(a) presents the measured R, G and B values of the artificial serum samples with K^+ ion concentrations ranging from 0.05–9 mM under the above optimal parameter conditions. All three color signals have good linearity (average determination coefficient $R^2 = 0.99$) over the considered K^+ ion concentration range. In other words, all three color components have a good correlation with the color development of the detection zone, while the corresponding sensitivities are 0.39 (R), 0.22 (G) and 0.31 (B) mM/a.u., respectively. ((i.e., [(9 − 0.1) mM]/[(177.2 − 154.3) a.u.] = 0.39 mM/a.u.). To obtain the optimized sensitivity in the permutation and combination of R, G and B, when R + G + B has a good linear relationship, it has an optimal sensitivity. Fig. 5(b) shows the results obtained when plotting the mean R + G+B values of the five samples against the K^+ ion concentration in the range of 0.05–9 mM. Notably, the determination coefficient between the mean R + G+B values and the K^+ ion concentration ($R^2 = 0.994$ and sensitivity = 0.10 mM/a.u.) is higher than that of any of the individual R, G and B signals in Fig. 5(a). In other words, the feasibility of

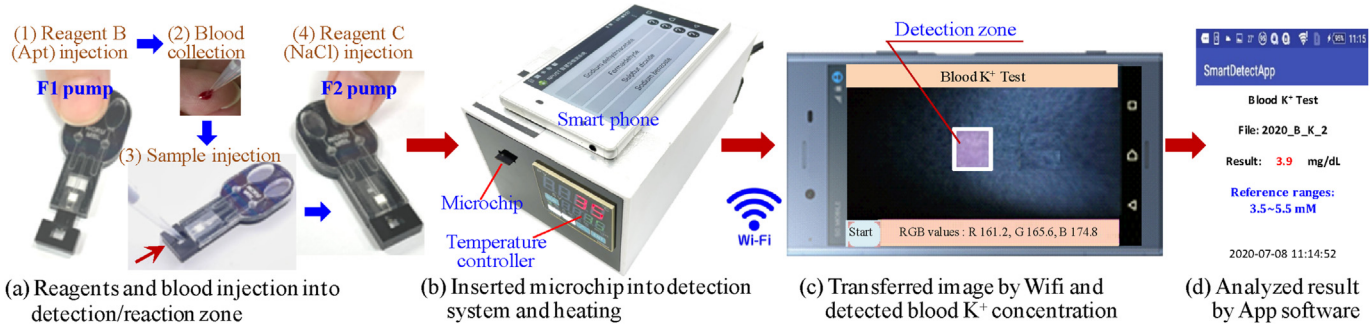

Fig. 2. The operating steps of the experimental procedure.

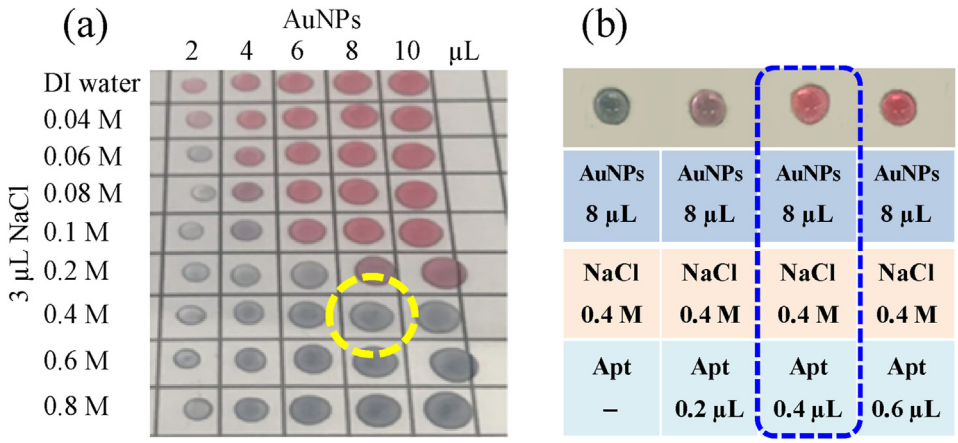

Fig. 3. (a) Reaction color for different volumes of AuNPs and concentrations of 3 μL NaCl. (b) Reaction color for 8 μL AuNPs, 3 μL NaCl (0.4 M) and different volumes of aptamers. (For interpretation of the references to color in this figure legend, the reader is referred to the Web version of this article.)

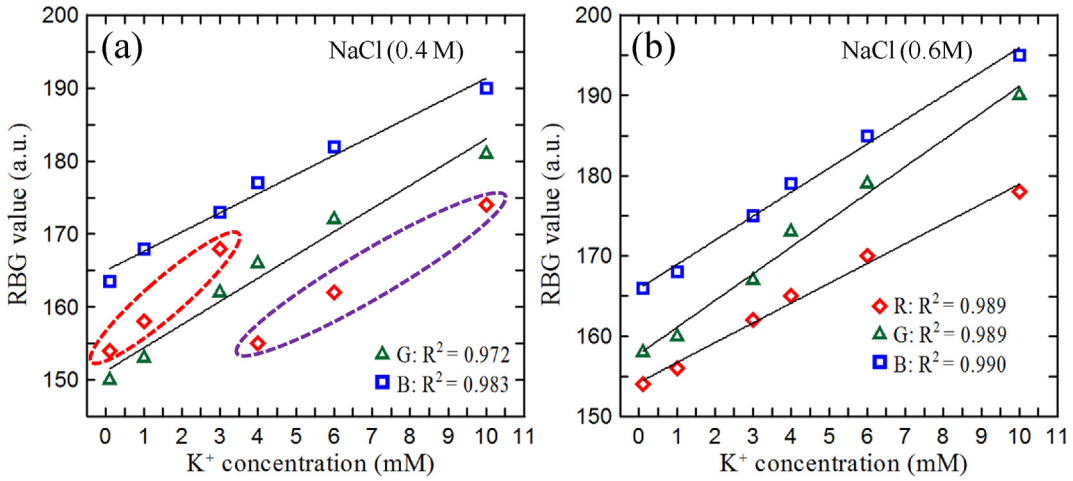

Fig. 4. The measured RGB value as function of K+ ion concentration (0.05–10 mM) given fixed parameter conditions of 8 μL AuNPs, 0.4 μL Apt and 3 μL NaCl. (a) NaCl concentration 0.4 M, and (b) NaCl concentration 0.6 M.

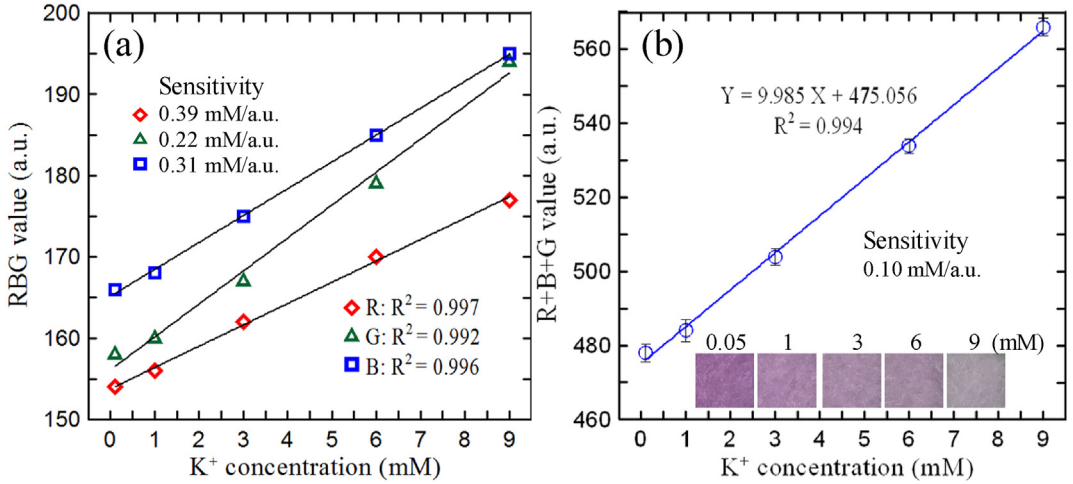

Fig. 5. (a) The measured RGB value as function of K^+ ion concentration (0.05–9 mM). (b) Total R + G+B value as function of K^+ ion concentration (0.05–9 mM).

using the total R + G+B value of the detection zone to quantify the K^+ ion concentration in the normal K^+ ion concentration range is confirmed. A detailed inspection of the RGB intensity measurements shows that the R + G + B value (Y) is related to the K^+ ion

concentration (X) by the relationship Y = 9.985 X + 475.056. In addition, the LOD of the proposed device was confirmed to be 0.01 mM in artificial serum.

3.2. Specificity of microfluidic aptasensor device for K^+ ion detection

Human serum contains many different electrolyte ions, the main ions are sodium (Na^+, reference value 135–145 mM), chloride (Cl^-, reference value 98–108 mM), calcium (Ca^{2+}, reference value 8.5–10.1 mM), potassium (K^+, reference value 3.5–5.5 mM), magnesium (Mg^{2+}, reference value 0.78–1.11 mM) and phosphorus (P, reference value 0.81–1.45 mM). Therefore, although the microfluidic aptasensor device in the current study is specially developed for measuring of K^+ ion concentration, its response to Na^+, Cl^-, Ca^{2+}, Mg^{2+} and P ions must also be considered. In order to evaluate the specificity of the microfluidic aptasensor device blood potassium detection, colorimetric reactions were performed using DI water (background), K^+ (3 mM), Na^+ (140 mM), Cl^- (110 mM), Ca^{2+} (10 mM), Mg^{2+} (2 mM) and P (2 mM). Note that the background R + G + B value represents the reaction value of reagents A, B and C with DI water. As shown in Fig. 6, none of electrolytes other than the K^+ ion with a concentration of 3 mM showed a strong color reaction. The R+G + B value of the phosphorus sample is around 7.6% higher than that of the background value. By contrast, the R + G + B values of the other ion samples are no more than 1% than that of the background value. In other words, the specificity of the AuNPs aptasensor for K^+ ions sample is confirmed.

3.3. Actual patient samples

The practical feasibility of the current PMMA/paper-based device is evaluated by comparing the K^+ ion concentration detection results obtained for 150 CKD patients with a total of 137 blood samples and 287 serum samples at National Cheng Kung University Hospital (NCKUH) with those obtained using an ion-selective electrodes (ISE) method (cobas® 8000 modular analyzer series, USA). Blood specimens were collected on four separate occasions, namely 2020/07/08 (50 patients, serum), 2020/10/15 (50 patients, blood/serum), 2020/11/12 (17 patients, blood/serum) and 2020/12/10 (50 patients, blood/serum). Calibration curve for current microfluidic aptasensor device was constructed using artificial serum samples, as described the previous section. The K^+ ion concentrations of the collected samples were then determined by substituting the total R+G + B intensity (microfluidic aptasensor device) into the calibration equations. The PMMA/paper-microchips required for the testing process were prepared 2 days before the first sample collection date and were stored in nitrogen at 4 °C.

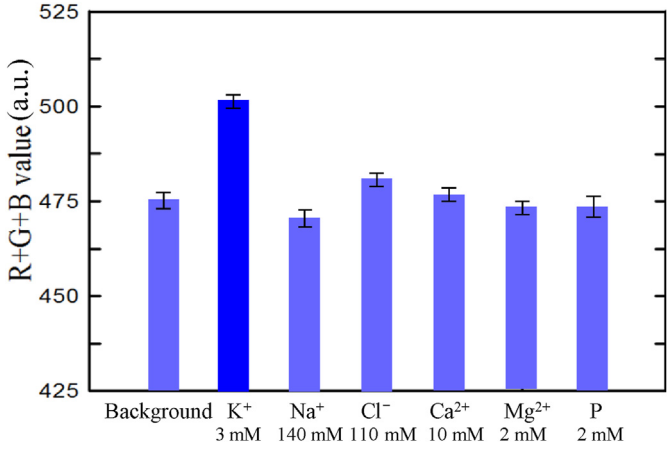

Fig. 6. R + G + B values of different electrolyte ions after reaction with the AuNPs aptasensor.

Fig. 7(a) shows the detection results obtained by the current microfluidic aptasensor method and NCKUH detection method (ISE method) for the 50 samples collected on 2020/10/15. From a detailed inspection, the recovery rate of the 50 samples is 96.2%, while the standard deviation is 5.4%. Moreover, a good qualitative agreement is observed between the two sets of results for all of the samples.

Following an analysis of the 50 samples collected on 2020/10/15, 17 patients with high serum K^+ ion concentrations (>5 mM) were selected to undergo oral hygiene education, adjustment of medication, dietary change, and prescribed rest for a period of 4 weeks. New samples were then collected from these patients on 2020/11/20. The detection results presented in Fig. 7(b) show that the K^+ ion concentration values of all 17 patients lie within the normal range following intervention. In addition, a good agreement is observed once again between the two sets of detection results. The results confirm that the current microfluidic aptasensor device can be used to monitor the serum K^+ ion concentration of CKD patients over time.

To evaluate the reliability of the microfluidic system after prolonged storage (58 days) blood samples were acquired from a further 50 CKD patients at NCKUH on 2020/12/10. Fig. 7(c) shows the corresponding detection results obtained by the proposed method and NCKUH detection method, respectively. A detailed inspection shows that the recovery rate of the 50 samples is 97.1%, while the standard deviation is 5.1%. In addition, a good agreement is observed between the two sets of results for all 50 samples. Consequently, the feasibility of the proposed PMMA/paper-microchip storage method (nitrogen, 4 °C) is confirmed. It is seen that the K^+ ion concentrations of the 50 samples all lie within the range of 3.5–6.0 mM. To evaluate the detection performance of the current microfluidic aptasensor device at lower (less than 3 mM and higher (greater than 6 mM) concentrations, 20 of the 50 samples shown in Fig. 7(c) were randomly selected and their K^+ ion concentrations decreased or increased accordingly. In particular, 10 samples were diluted by a factor of 2.5-times through the addition of DI water, while 10 samples were mixed with K^+ ion concentrations of 2.5 mM to increase their concentration by a corresponding amount. The detection results for the 20 samples are shown in Fig. 7(d). It is seen that the results obtained using the current microfluidic aptasensor device are still consistent with those obtained using the NCKUH detection method. The results confirm that the current microfluidic aptasensor device has the ability to measure K^+ ion concentration in a wide clinical range.

Fig. 8(a) and (b) show a scatter plot of the results acquired by the current microfluidic aptasensor device and NCKUH testing system, respectively, for all 137 whole blood and 287 serum samples. As shown, the determination coefficient (R^2) between the two sets of results is 0.968 and 0.980, respectively. Note that in order to present the applicability of the detection range of the current microfluidic aptasensor POC device, the 50 samples (serum) collected on 2020/07/08 were diluted 1.5 times (25 samples) and 2.5 times (25 samples), and the 50 samples (serum) collected on 2020/10/15 were mixed with K^+ ion concentrations of 1.5 mM (25 samples) and 2.5 mM (25 samples) to increase the concentration by a corresponding amount. The corresponding results are shown in Fig. 8(b). Table 1 presents comparisons of several properties between the current microfluidic aptasensor device and the developed methods for K^+ ion detection in human samples. Overall, the results presented in Fig. 8 confirm that the current microfluidic aptasensor

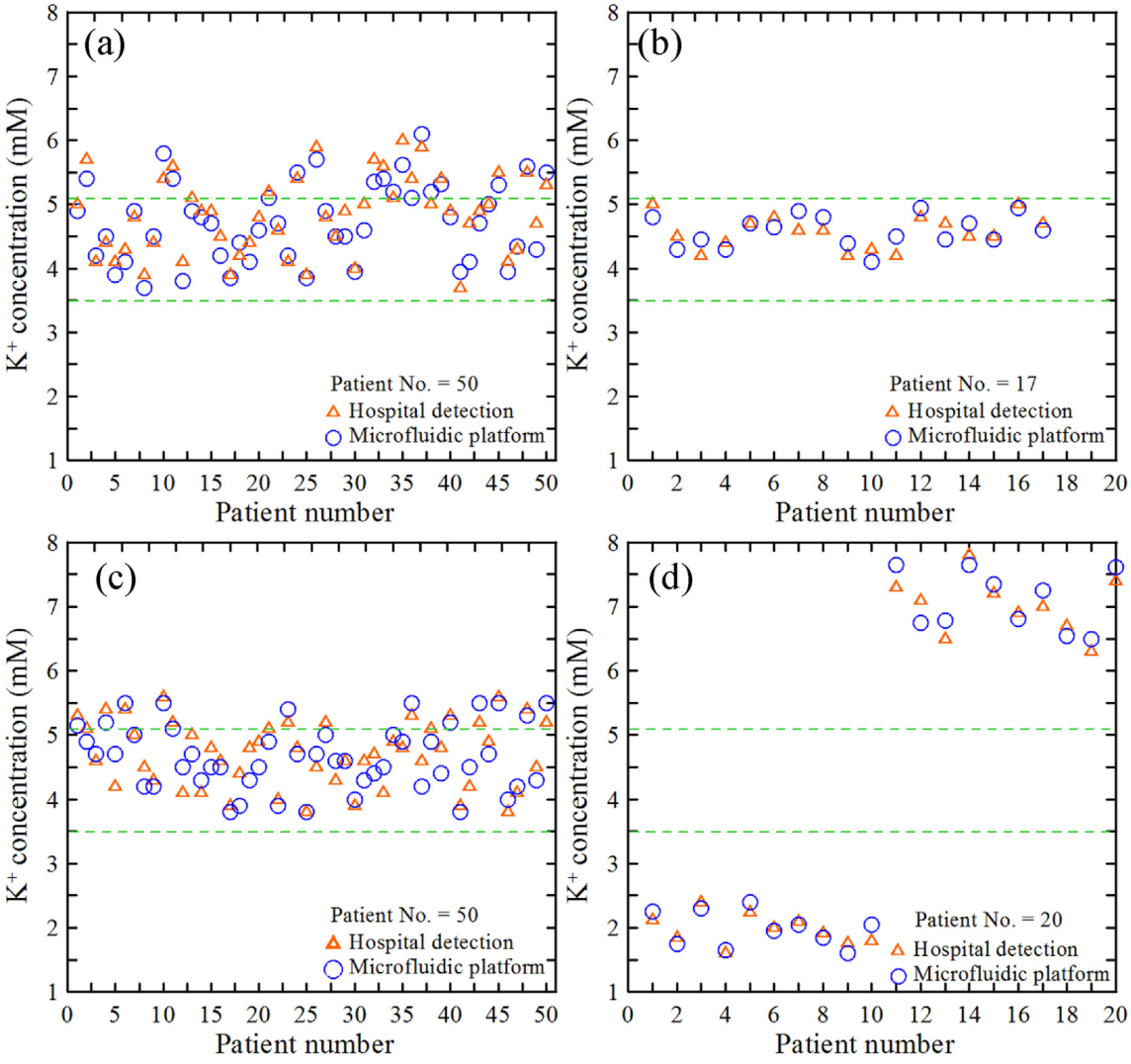

Fig. 7. Comparison of K^+ ion detection results acquired using current microfluidic aptasensor platform and ISE method, respectively. (a) 50 samples collected on 2020/10/5 (b) 17 samples collected on 2020/11/12, (c) 50 samples collected on 2020/12/10, and (d) 20 samples collected on 2020/12/10 and subsequently diluted or concentrated.

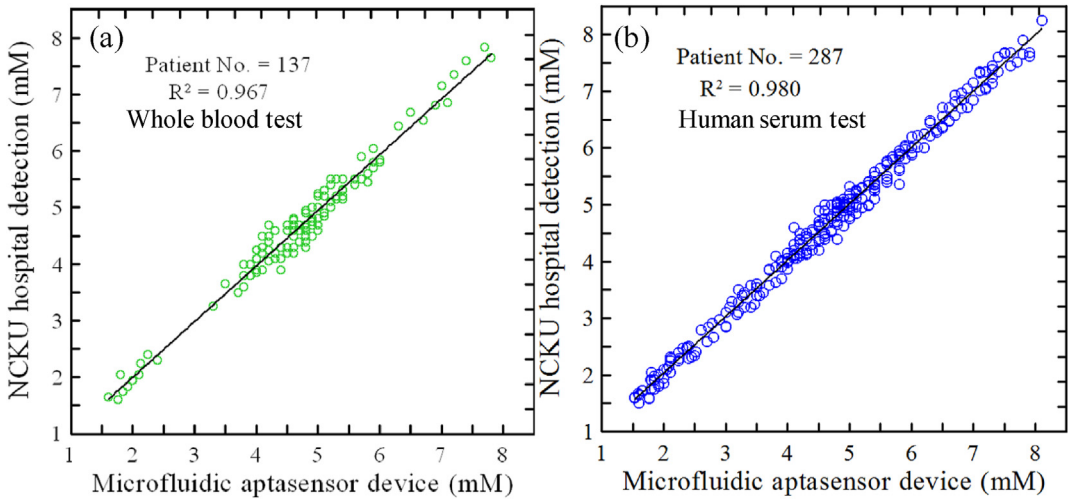

Fig. 8. Correlation between K^+ ion concentration results acquired using current microfluidic aptasensor device and NCKU Hospital detection method.

Table 1
Comparison of several properties between the current microfluidic aptasensor device and the developed methods for K^+ ion detection in human samples.

Author and year	Sample type and pretreatment	Real samples	Detection method and system	Reagent	Detection range	LOD	Ref.
Current system	Whole blood, Non-pretreatment	137	Microchip + Colorimetric Handheld	Aptamer + AuNPs	0.05–9 mM	0.01 mM	–
NCKU hospital	Serum, Centrifugal	–	ISE method Benchtop	–	0.5–10 mM	–	–
Braiek et al., 2016	Whole blood, Dilute, Centrifugal	3	Conductometric method Benchtop	Ion-selective membrane	0.1–16 mM	0.1 mM	[61]
Su et al., 2016	Serum, Centrifugal	1	RS spectroscopy Benchtop	Sodium cobaltinitrite	0.01–50 mM	0.01 mM	[6]
Du and Xie 2017	Plasma, –	No.	ISOs method Benchtop	Agarose hydrogel	0.1–100 mM	0.1 mM	[7]
Liu et al., 2017	Serum, Centrifugal	5	OES method Benchtop	Cation exchange membrane	0.51–17.92 mM	0.15 mM	[62]
Kollegger et al., 2018	Whole blood, –	No.	Potentiometric method Handheld	Ion-selective membrane	1–10 mM	1 mM	[63]
Gul et al., 2019	Serum –	No.	Potentiometric method Benchtop	Dibenzo-18-crown-6	3–5 mM	3 mM	[64]
Shen et al., 2019	Serum, Centrifugal	3	Fluorescence Benchtop	Cyanine dye & oligonucleotides	0.01–4.5 mM	0.01 mM	[65]
Zhao et al., 2020	Whole blood, Dilute	7	CE-C^4D Benchtop	MES	50–5000 μM	14.9 μM	[9]
Naderi et al., 2018	Urine, Dilute	4	μPAD + Colorimetric Handheld	Aptamer + AuNPs	0.01–40 mM	6.2 μM	[66]
Qiu et al., 2019	Urine, Centrifugal	3	UV spectrophotometry Benchtop	ABC + AuNPs	0–0.2 mM	40 μM	[8]
Surendran et al., 2019	Saliva, Dilute	3	Microchip + Optical Benchtop	Benedict's reagent	–	–	[67]

ABC: 4-aminobenzo-18-crown-6; C^4D: Capacitively coupled contactless conductivity detector; ISOs: Ion-selective optodes (ISOs); MES: Morpholine ethane sulfonic acid; OES: Optical emission spectrometric; RS: Raman scattering; μPAD: Microfluidic paper-based device.

device provides a reliable and accurate approach for detecting the serum K^+ concentration of real-world CKD patients.

4. Conclusion

This study has proposed a microfluidic AuNP/aptamer sensor device for determining the whole blood K^+ concentration of CKD patients. In the proposed device, an AuNP aptasensor is prepared on the detection zone of a paper-chip and subsequently reacts with K^+ ions in the serum sample after separation of whole blood to produce a rigid G-quadruplex structure. The formation of this structure results in the release of some of the AuNPs from the aptasensor in a quantity proportional to the K^+ ion concentration. The released AuNPs aggregate under the effects of NaCl reagent and produce a color change of the detection zone from which the K^+ ion concentration is then used RGB analysis app software. The proposed device is shown to achieve a good linear response ($R^2 = 0.994$) for artificial serum samples with known K^+ concentrations in the range of 0.05–9 mM. Moreover, the test results of 137 real-world CKD whole blood and 287 serum samples and the results obtained using the ion-selective electrode method showed excellent agreement ($R^2 = 0.968$ and $R^2 = 0.980$). The currently developed microfluidic aptamer sensor device was easy to produce and can be used as a low-cost home self-monitoring device, with a price of less than US$ 0.50 per microchip. In the future, CKD patients will be provided with a simple, fast, accurate and reliable self-monitoring method of K^+ ion concentration in whole blood.

CRediT authorship contribution statement

Chin-Chung Tseng: Data curation, Writing – original draft, Supervision. **Song-Yu Lu:** Investigation, Methodology, Software, Data curation, Writing – review & editing, Investigation. **Szu-Jui Chen:** Investigation, Methodology, Software, Data curation, Writing – review & editing, Investigation. **Ju-Ming Wang:** Writing – review & editing, Investigation. **Lung-Ming Fu:** Data curation, Writing – original draft, Supervision. **Yi-Hong Wu:** Writing – review & editing, Investigation.

Declaration of competing interest

The authors declare that they have no known competing financial interests or personal relationships that could have appeared to influence the work reported in this paper.

Acknowledgement

The authors would like to thank the Ministry of Science and Technology of Taiwan for the financial support of this study under Grant Nos. MOST 106-2314-B-006-085 -MY3, MOST 106-2221-E-006-253-MY3, MOST 107-2622-B-006-007-CC2, and MOST 106TFDA-A-103.

Appendix A. Supplementary data

Supplementary data to this article can be found online at https://doi.org/10.1016/j.aca.2022.339722.

Appendix

文件編號：8800-4-07-001
表單編號：表單 58

Institutional Review Board
National Cheng Kung University Hospital
138 Sheng-Li Rd, Tainan 704, Taiwan R.O.C.
TEL:886-6-2353535 ext.3635 FAX:886-6-2388190

國立成功大學醫學院附設醫院 A063h
第一人體研究倫理審查委員會
台灣.台南市勝利路138號
E-mail:em73635@mail.hosp.ncku.edu.tw

Human Study Approval

Date: 2017.02.07

Title: Rapid-Detection of creatinine, blood erea nitrogen, glucose, albumin, total protein and potassium in Human Blood/Urine Using Paper-Based Chips and Smartphone Reader.

Protocol No/ IRB No: --/ A-ER-105-503

Period of Project: From 2017.01.26 to 2020.12.31

Period of Approval: From 2017. 01.26 to 2018. 01.25

Content/Version:

1. Protocol: Version: 1 , Date: 2016.12.28
2. Informed Consent Form: Version: 2, Date: 2016.01.24

Institute: National Cheng Kung University Hospital
Investigator: Dr. Chin-Chung Tseng (Department of Internal Medicine)
Co-Investigators: Postdoctoral Fellow Wei-Jhong Ju

Approved Number of Participants: NCKUH 200 Persons. If the number of participants enrolled exceeds the approved number, please submit an application for amendment and approval.

The Institutional Review Board of National Cheng Kung University Hospital (NCKUH) is organized and operated according to the laws and regulations of ICH-GCP and of Central Competent Authorities.

This project is reviewed and approved by NCKUH IRB in 2017.01.26. The period of approval is granted until 2018. 01.25.

Regarding multi-period project, please submit the Interim Report before 2017.12.25. If the approval of the interim report is not granted on its expiry date, except safeguarding the health of the participants, the research is suspended.

Regarding completed project, the Final Report shall be submitted within three months of its approved expiry date. Except for the health of the participants, all the procedures of the project shall be terminated on its approved stated deadline.

If PI does not submit the Interim/Final Report on time, he/she will be recorded in the overdue list and received the suspension/ termination notice from NCKUH IRB. The overdue list will be reported to the IRB. After the resolution of the board meeting, NCKUH IRB will suspend all the new projects applied by PI until the Interim/Final Report is submitted.

Please submit the Interim/Final Report in written form and send to NCKUH IRB office. The lastest application forms can be downloaded in its website (http：// www.ncku.edu.tw/ ~nckuhirb)

Any changes or amendments to the project (including the project period), please submit an amendment application to NCKUH IRB within its approved period. Any changes or amendments in any other way will not be accepted. Before the approval of the amendment application, the project is carried out according to its previously approved plan.

For some reasons projects granted approval by NCKUH IRB couldn't be implemented, PI shall apply for suspension/termination.

During or after the project is completed, please report any unfavorable occurrence in a human study particant according to GCP.

Yours sincerely,
Thy-Sheng Lin M.D.
Chairman Thy-Sheng Lin

Institutional Review Board
National Cheng Kung University Hospital

經第 B053 次大會通過版

References

[1] S. Antwi-Baffour, J.K. Adjei, F. Tsyawo, R. Kyeremeh, F.A. Botchway, M.A. Seidu, A study of the change in sodium and potassium ion concentrations in stored donor blood and their effect on electrolyte balance of recipients, BioMed Res. Int. 2019 (2019) 8162975.

[2] M. Tarik, L. Ramakrishnan, R. Amarchand, H.R. Salve, P. Mathur, P. Joshi, A. Krishnan, Feasibility of measuring sodium, potassium and creatinine from urine sample dried on filter paper, Bioanalysis 11 (2019) 689–701.

[3] L. Yang, Z. Qing, C. Liu, Q. Tang, J. Li, S. Yang, J. Zheng, R. Yang, W. Tan, Direct fluorescent detection of blood potassium by ion-selective formation of intermolecular G-quadruplex and ligand binding, Anal. Chem. 88 (2016) 9285–9292.

[4] Q. Yuan, S. Wu, C. Ye, X. Liu, J. Gao, N. Cui, P. Guo, G. Lai, Q. Wei, M. Yang, Sensitivity enhancement of potassium ion (K^+) detection based on graphene field-effect transistors with surface plasma pretreatment, Sensor. Actuator. B Chem. 285 (2019) 333–340.

[5] Y.Q. Kondratyeva, E.G. Tolstopjatova, D.O. Kirsanov, K.N. Mikhelson, Chronoamperometric and coulometric analysis with ionophore-based ion-selective electrodes: a modified theory and the potassium ion assay in serum samples, Sensor. Actuator. B Chem. 310 (2020) 127894.

[6] H. Su, W. Ruan, S. Ye, Y. Liu, H. Sui, Z. Li, X. Sun, C. He, B. Zhao, Detection of physiological potassium ions level in human serum by Raman scattering spectroscopy, Talanta 161 (2016) 743–747.

[7] X. Du, X. Xie, Non-equilibrium diffusion controlled ion-selective optical sensor for blood potassium determination, ACS Sens. 2 (2017) 1410–1414.

[8] J. Qiu, Y. Zhang, C. Dong, Y. Huang, L. Sun, H. Ruan, H. Wang, X. Li, A. Wu, Rapid colorimetric detection of potassium ions based on crown ether modified Au NPs sensor, Sensor. Actuator. B Chem. 281 (2019) 783–788.

[9] L. Zhao, F. Luo, A. Wang, J. Zhang, Y. Wang, L. Zhao, Z. Wang, Q. Pu, Quick stabilization of capillary for rapid determination of potassium ions in the blood of epilepsy patients by capillary electrophoresis without sample pretreatment, Electrophoresis 41 (2020) 1273–1279.

[10] M.P. Jewell, M.D. Greer, A.L. Dailey, K.J. Cash, Triplet-triplet annihilation upconversion based nanosensors for fluorescence detection of potassium, ACS Sens. 5 (2020) 474–480.

[11] L.A.N. Dayao, C.C. Liu, S.Y. Hsu, L.L. Tayo, W.J. Ju, L.M. Fu, Multifunctional microchip-based distillation apparatus II-Aerated distillation for sulfur dioxide detection, Anal. Chim. Acta 1071 (2019) 44–52.

[12] S.Y. Hsu, C.C. Liu, C.E. Yang, L.M. Fu, Multifunctional microchip-based distillation apparatus I-Steam distillation for formaldehyde detection, Anal. Chim. Acta 1062 (2019) 94–101.

[13] P.F. Xu, Z.H. Liu, Q. Sun, D. Wang, X.F. Zeng, J.X. Wang, Microfluidic controllable synthesis of monodispersed sulfur nanoparticles with enhanced antibacterial activities, Chem. Eng. J. 398 (2020) 125293.

[14] H. Lee, M.T. Oh, Y.J. Lee, K.H. Son, N. Choi, B.C. Lee, S.H. Lee, Highly-efficient microfluidic ultrasonic transducers assisted gDNA extraction system in whole blood for POCT applications, Sensor. Actuator. B Chem. 319 (2020) 128317.

[15] C.C. Tseng, S.J. Chen, S.Y. Lu, C.H. Ko, J.M. Wang, L.M. Fu, Y.H. Liu, Novel sliding hybrid microchip detection system for determination of whole blood phosphorus concentration, Chem. Eng. J. 419 (2021) 129592.

[16] C.T. Kung, H. Gao, C.Y. Lee, Y.N. Wang, W. Dong, C.H. Ko, G. Wang, L.M. Fu, Microfluidic synthesis control technology and its application in drug delivery, bioimaging, biosensing, environmental analysis and cell analysis, Chem. Eng. J. 399 (2020) 125748.

[17] Y.T. Wu, C.E. Yang, C.H. Ko, Y.N. Wang, C.C. Liu, L.M. Fu, Microfluidic detection platform with integrated micro-spectrometer system, Chem. Eng. J. 393 (2020) 124700.

[18] N.R. Victor, B. Dennis, W. Hess, Flow control in fully enclosed microfluidics paper based analytical devices using plasma processes, Sensor. Actuator. B Chem. 320 (2020) 128606.

[19] A. Zizzari, M. Cesari, M. Bianco, L.L. del Mercato, M. Carraro, M. Bonchio, R. Rella, V. Arima, Mixing enhancement induced by viscoelastic micromotors in microfluidic platforms, Chem. Eng. J. 391 (2020) 123572.

[20] C.J.D. Laurenciano, C.C. Tseng, S.J. Chen, S.Y. Lu, L.L. Tayo, L.M. Fu, Microfluidic colorimetric detection platform with sliding hybrid PMMA/paper microchip for human urine and blood sample analysis, Talanta 228 (2021) 122362.

[21] G.C. Rezende, S. Le Calvé, J.J. Brandner, D. Newport, Characterization of a modular microfluidic photoionization detector, Sensor. Actuator. B Chem. 324 (2020) 128667.

[22] C. Wu, G. Gao, K. Zhai, L. Xu, D. Zhang, A visual Hg^{2+} detection strategy based on distance as readout by G-quadruplex DNAzyme on microfluidic paper, Food Chem. 331 (2020) 127208.

[23] J. Yang, Y. Zhu, F. Wang, L. Deng, X. Xu, W. Cui, Microfluidic liposomes-anchored microgels as extended delivery platform for treatment of osteoarthritis, Chem. Eng. J. 400 (2020) 126004.

[24] J.H. Lin, T.T. Tsai, Q. Zeng, C.Y. Chang, J.Y. Guo, C.J. Lin, C.F. Chen, A multifunctional microfluidic device for blood typing and primary screening of blood diseases, ACS Sens. 5 (2020) 3082–3090.

[25] T. Jaouhari, F. Zhang, T. Tassaing, S. Fery-Forgues, C. Aymonier, S. Marre, A. Erriguible, Process intensification for the synthesis of ultra-small organic nanoparticles with supercritical CO_2 in a microfluidic system, Chem. Eng. J. 397 (2020) 125333.

[26] P.F. Xu, Z.H. Liu, Y.H. Duan, Q. Sun, D. Wang, X.F. Zeng, J.X. Wang, Microfluidic controllable synthesis of monodispersed sulfur nanoparticles with enhanced antibacterial activities, Chem. Eng. J. 398 (2020) 125293.

[27] L. Vobecká, L. Tichá, A. Atanasova, Z. Slouka, P. Hasal, M. Přibyl, Enzyme synthesis of cephalexin in continuous-flow microfluidic device in ATPS environment, Chem. Eng. J. 396 (2020) 125236.

[28] F. Huang, R. Guo, L. Xue, G. Cai, S. Wang, Y. Li, M. Liao, M. Wang, J. Lin, An acid-responsive microfluidic salmonella biosensor using curcumin as signal reporter and ZnO-capped mesoporous silica nanoparticles for signal amplification, Sensor. Actuator. B Chem. 312 (2020) 127958.

[29] H. Daguerre, M. Solsona, J. Cottet, M. Gauthier, P. Renaudb, A. Bolopion, Positional dependence of particles and cells in microfluidic electrical impedance flow cytometry: origin, challenges and opportunities, Lab Chip 20 (2020) 3665–3689.

[30] X. Wei, Y. Lu, X. Zhang, M.L. Chen, J.H. Wang, Recent advances in single-cell ultra-trace analysis, Trac. Trends Anal. Chem. 127 (2020) 115886.

[31] L.M. Fu, Y.N. Wang, Detection methods and applications of microfluidic paper-based analytical devices, Trac. Trends Anal. Chem. 107 (2018) 196–211.

[32] Y. Gong, Y. Zheng, B. Jin, M. Youa, J. Wang, X. Li, M. Lin, F. Xu, F. Li, A portable and universal upconversion nanoparticle-based lateral flow assay platform for point-of-care testing, Talanta 201 (2019) 126–133.

[33] C.T. Kung, C.Y. Hou, Y.N. Wang, L.M. Fu, Microfluidic paper-based analytical devices for environmental analysis of soil, air, ecology and river water, Sensor. Actuator. B Chem. 301 (2019) 126855.

[34] Q. Huang, K. Zhang, Y. Yang, J. Ren, R. Sun, F. Huang, X. Wang, Highly smooth, stable and reflective Ag-paper electrode enabled by silver mirror reaction for organic optoelectronics, Chem. Eng. J. 370 (2019) 1048–1056.

[35] H.Y. Ng, W.C. Lee, C.T. Kung, L.C. Li, C.T. Lee, L.M. Fu, Recent advances in microfluidic devices for contamination detection and quality inspection of milk, Micromachines 12 (2021) 558.

[36] M. Taghizadeh-Behbahani, B. Hemmateenejad, M. Shamsipur, A. Tavassoli, A paper-based length of stain analytical device for naked eye (readout-free) detection of cystic fibrosis, Anal. Chim. Acta 1080 (2019) 138–145.

[37] L.P. Murray, C.R. Mace, Usability as a guiding principle for the design of paper-based, pointof-care devices - a review, Anal. Chim. Acta 1140 (2020) 236–249.

[38] R.J. Yang, C.C. Tseng, W.J. Ju, H.L. Wang, L.M. Fu, A rapid paper-based detection system for determination of human serum albumin concentration, Chem. Eng. J. 352 (2018) 241–246.

[39] W.C. Lee, H.Y. Ng, C.Y. Hou, C.T. Lee, L.M. Fu, Recent advances in lab-on-paper diagnostic devices using blood samples, Lab Chip 21 (2021) 1433–1453.

[40] C.C. Tseng, C.T. Kung, R.F. Chen, M.H. Tsai, H.R. Chao, Y.N. Wang, L.M. Fu, Recent advances in microfluidic paper-based assay devices for diagnosis of human diseases using saliva, tears and sweat samples, Sensor. Actuator. B Chem. 342 (2021) 130078.

[41] F. Li, M. You, S. Li, J. Hu, C. Liu, Y. Gong, H. Yang, F. Xu, Paper-based point-of-care immunoassays: recent advances and emerging trends, Biotechnol. Adv. 39 (2020) 107442.

[42] E. Noviana, D.B. Carrão, R. Pratiwi, C.S. Henry, Emerging applications of paper-based analytical devices for drug analysis: a review, Anal. Chim. Acta 1116 (2020) 70–90.

[43] B.S. Batule, Y. Seok, M.G. Kim, An innovative paper-based device for DNA extraction from processed meat products, Food Chem. 321 (2020) 126708.

[44] C.Y. Hou, L.M. Fu, W.J. Ju, P.Y. Wu, Microfluidic colorimetric system for nitrite detection in foods, Chem. Eng. J. 398 (2020) 125573.

[45] C.C. Tseng, C.H. Ko, S.Y. Lu, C.E. Yang, L.M. Fu, C.Y. Li, Rapid electrochemical-biosensor microchip platform for determination of microalbuminuria in CKD patients, Anal. Chim. Acta 1146 (2021) 70–76.

[46] R. Caoa, Z. Panb, H. Tang, J. Wu, J. Tianc, A. Nilghazd, M. Li, Understanding the coffee-ring effect of red blood cells for engineering paper-based blood analysis devices, Chem. Eng. J. 391 (2020) 123522.

[47] I. Lewińska, M. Speichert, M. Granica, Ł. Tymecki, Colorimetric point-of-care paper-based sensors for urinary creatinine with smartphone readout, Sensor. Actuator. B Chem. 340 (2021) 129915.

[48] W.C. Lee, H.Y. Ng, C.Y. Hou, C.T. Lee, L.M. Fu, Recent advances in lab-on-paper diagnostic devices using blood samples, Lab Chip 21 (2021) 1433–1453.

[49] Y. Cai, J.C. Niu, Y.Q. Liu, X.L. Du, Z.Y. Wu, Online sample clean-up and enrichment of proteins from salty media with dynamic double gradients on a paper fluidic channel, Anal. Chim. Acta 1100 (2020) 149–155.

[50] J. Chen, H. Li, H. Xie, D. Xu, A novel method combining aptamer-Ag_{10}NPs based microfluidic biochip with bright field imaging for detection of KPC-2-expressing bacteria, Anal. Chim. Acta 1132 (2020) 20–27.

[51] H. Liu, P. Zhao, Y. Wang, S. Li, L. Zhang, Y. Zhang, S. Ge, J. Yu, Paper-based sandwich type SERS sensor based on silver nanoparticles and biomimetic recognizer, Sensor. Actuator. B Chem. 313 (2020) 127989.

[52] S.P. Huang, Y.J. Chuang, W.B. Lee, Y.C. Tsai, C.N. Lin, K.F. Hsu, G.B. Lee, An integrated microfluidic system for rapid, automatic and high-throughput staining of clinical tissue samples for diagnosis of ovarian cancer, Lab Chip 20 (2020) 1103–1109.

[53] K. Pungjunun, S. Nantaphol, N. Praphairaksit, W. Siangproh, S. Chaiyo, O. Chailapakul, Enhanced sensitivity and separation for simultaneous determination of tin and lead using paper-based sensors combined with a portable potentiostat, Sensor. Actuator. B Chem. 318 (2020) 128241.

[54] T. Bhardwaj, P. Dalal, A.S. Rathore, S.K. Jha, An aptamer based microfluidic chip for impedimetric detection of Ranibizumab in a bioreactor, Sensor. Actuator. B Chem. 312 (2020) 127941.

[55] T. Li, G. Ou, X. Chen, Z. Li, R. Hu, Y. Li, Y. Yang, M. Liu, Naked-eye based point-

of-care detection of E. coli O157: H7 by a signal amplified microfluidic aptasensor, Anal. Chim. Acta 1130 (2020) 20–28.
[56] V. Singh, Ultrasensitive quantum dot-coupled-surface plasmon microfluidic aptasensor array for serum insulin detection, Talanta 219 (2020) 121314.
[57] K. Xing, J. Peng, W. Chen, B. Fang, D. Liu, S. Shan, G. Zhang, Y. Huang, W. Lai, Development of a label-free plasmonic gold nanoparticles aggregates sensor on the basis of charge neutralization for the detection of zearalenone, Food Chem. 370 (2022) 131365.
[58] D. Li, Z. Luo, H. An, E. Yang, M. Wu, Z. Huang, Y. Duan, Poly-adenine regulated DNA density on AuNPs to construct efficient DNA walker for microRNA-21 detection, Talanta 217 (2020) 121056.
[59] T.F. Hong, W.J. Ju, M.C. Wu, C.H. Tsai, L.M. Fu, Rapid prototyping of PMMA microfluidic chips utilizing a CO_2 laser, Microfluid. Nanofluidics 9 (2010) 1125–1133.
[60] L.M. Fu, W.J. Ju, Y.N. Wang, R.J. Yang, Prototyping of glass-based microfluidic chips utilizing two-pass defocused CO_2 laser beam method, Microfluid. Nanofluidics 14 (2013) 479–487.
[61] M. Braiek, M.A. Djebbi, J.F. Chateaux, N. Jaffrezic-Renault, A conductometric sensor for potassium detection in whole blood, Sensor. Actuator. B Chem. 235 (2016) 27–32.
[62] S. Liu, Y. Cai, Y.L. Yu, J.H. Wang, A miniature liquid electrode discharge-optical emission spectrometric system integrating microelectrodialysis for potassium screening in serum, J. Anal. At. Spectrom. 32 (2017) 1739–1745.
[63] C. Kollegger, P. Greiner, I. Siegl, C. Steffan, M. Wiessflecker, B. Pekec, M. Hajnsek, F. Sinner, G. Holweg, B. Deutschmann, Intelligent NFC potassium measurement strip with hemolysis check in capillary blood, Elektrotechnik & Informationstechnik 135 (2018) 83–88.
[64] S. Gul, L. O'Neill, J. Cassidy, I. Naydenova, Modified surface relief layer created by holographic lithography: application to selective sodium and potassium sensing, Sensors 19 (2019) 1026.
[65] G. Shen, H. Zhang, J. Xiang, F. Yang, S. Wu, W. Wang, N. Du, J. Zhang, T. Sun, Y. Tang, Direct detection of potassium and lead (ii) ions based on assembly-disassembly of a chiral cyanine dye/tba complex, Talanta 201 (2019) 490–495.
[66] M. Naderi, M. Hosseini, M.R. Ganjali, Naked-eye detection of potassium ions in a novel gold nanoparticle aggregation-based aptasensor, Spectrochim. Acta, Part A 195 (2018) 75–83.
[67] V. Surendran, T. Chiulli, S. Manoharan, S. Knisley, M. Packirisamy, A. Chandrasekaran, Acoustofluidic micromixing enabled hybrid integrated colorimetric sensing, for rapid point-of-care measurement of salivary potassium, Biosensors 9 (2019) 73.